Towards an Efficient and Scalable Discontinuous Galerkin Atmospheric Model

J. M. Dennis[1,2], M. Levy[2], R. D. Nair[1], H. M. Tufo[1,2], and T. Voran[2]

Abstract

An efficient and scalable Discontinuous Galerkin shallow water model on the cubed sphere is developed by extending the transport scheme of Nair et al. [16]. The continuous flux form nonlinear shallow water equations in curvilinear coordinates are developed. Spatial discretization is a nodal basis set of Legendre polynomials. Fluxes along internal element interfaces are approximated by a Lax-Friedrichs scheme. A third-order total variation diminishing Runge-Kutta scheme is applied for time integration, without any filter or limiter. The standard shallow-water test suite of Williamson et al. [23] is used to validate the model. It is observed that the numerical solutions are accurate, the model conserves mass to machine precision, and there are no spurious oscillations in a test case where zonal flow impinges a mountain,. Development time was substantially reduced by building the model in the High Order Method Modeling Environment (HOMME) developed at the National Center for Atmospheric Research (NCAR). Performance and scaling data for the steady state geostrophic flow problem [23] is presented. Sustained performance in excess of 10% of peak is observed out to 64 processors on a Linux cluster.

keywords: discontinuous Galerkin method, climate and atmospheric modeling, parallel computing.

1 Introduction

High-order methods are becoming increasingly popular in atmospheric modeling. One such method, the spectral element (SE) method, has been adopted by several research groups to build the next generation of atmospheric models (see, e.g., [20, 21, 10, 7, 5]). Spectral elements have numerous attractive features such as exponential convergence, computational efficiency, scalability, and the ability to handle complex geometries. However, a major disadvantage of SE atmospheric models is a lack of conservation. For climate and atmospheric chemistry applications, conservation of integral invariants such as mass and energy as well as monotonicity of the solutions are crucial. To date there have been several efforts to develop conservative atmospheric models but they are all based on classic low-order finite-volume methods.

The high-order discontinuous Galerkin (DG) method is ideally suited for atmospheric numerical modeling because it is inherently conservative and can easily incorporate monotonic slope limiters. Moreover, it retains all the advantages of the SE method. The DG method is a hybrid approach combining the finite-volume and the finite-element methods, exploiting the merits of both. DG methods became popular following the work of Cockburn and Shu [1, 2, 3].

In this paper we present an overview of the DG shallow water model on the cubed-sphere developed by Nair et al. [16, 17], extend the model to employ a nodal basis set, present numerical results on the Williamson et al. [23] shallow water test suite, and show performance results for a selected test case.

2 Shallow Water Model on the Cubed-Sphere

As described in Nair et al. [16], the sphere is decomposed into six identical regions (Fig.1), obtained by central (gnomonic) projection of the faces of the inscribed cube onto the spherical surface [19, 18]. Each

[1]Scientific Computing Division, National Center for Atmospheric Research, 1850 Table Mesa Dr., Boulder, CO 80305, USA.
[2]Department of Computer Science, University of Colorado, Engineering Center - 430UCB, Boulder, CO 80309, USA.

of the six local coordinate systems is free of singularities and employ identical metric terms, creating a non-orthogonal curvilinear coordinate system on the sphere.

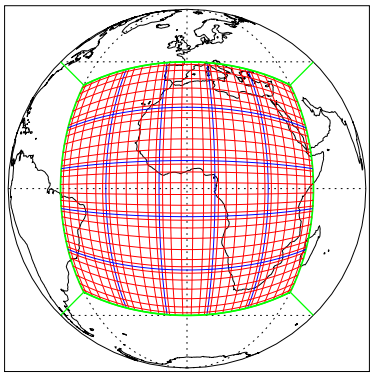

Figure 1: *A cubed-sphere with 25 elements ($N_e = 5$) on a face. 150 elements are required to span the surface of the sphere ($6 \times N_e^2 = 150$). Each element contains 8×8 Gauss-Lobatto-Legendre (GLL) points.*

Let $\mathbf{a}_1$ and $\mathbf{a}_2$ be the covariant base vectors of the transformation between inscribed cube and spherical surface. Let $\mathbf{v} = \mathbf{v}(\lambda, \theta)$ be the horizontal velocity vector specified on the sphere with longitude λ and latitude θ. Then, the components of the covariant vectors are given by $u_1 = \mathbf{v} \cdot \mathbf{a}_1$, $u_2 = \mathbf{v} \cdot \mathbf{a}_2$ and the corresponding contravariant components are expressed as $\mathbf{v} = u^1\,\mathbf{a}_1 + u^2\,\mathbf{a}_2$. The metric tensor of the transformation is defined as $G_{ij} \equiv \mathbf{a}_i \cdot \mathbf{a}_j$. Covariant and contravariant vectors are related through the metric tensor G_{ij} such that $u_i = G_{ij}u^j$, $u^i = G^{ij}u_j$, where $G^{ij} = (G_{ij})^{-1}$ and $G = \det(G_{ij})$. For equiangular coordinates (x^1, x^2), the metric tensor for all six faces of the cube is

$$G_{ij} = \frac{1}{r^4 \cos^2 x^1 \cos^2 x^2} \begin{bmatrix} 1 + \tan^2 x^1 & -\tan x^1 \tan x^2 \\ -\tan x^1 \tan x^2 & 1 + \tan^2 x^2 \end{bmatrix} = A^T A, \tag{1}$$

where $r = (1 + \tan^2 x^1 + \tan^2 x^2)^{1/2}$ and $\sqrt{G} = 1/r^3 \cos^2 x^1 \cos^2 x^2$. The matrix A in (1) can be used for transforming $\mathbf{v}$ with spherical velocity components (u, v) to the local cube-face components (u^1, u^2) and vice versa, as follows ([16]).

$$A \begin{bmatrix} u^1 \\ u^2 \end{bmatrix} = \begin{bmatrix} u \\ v \end{bmatrix}, \quad A = \begin{bmatrix} \cos\theta\, \partial\lambda/\partial x^1 & \cos\theta\, \partial\lambda/\partial x^2 \\ \partial\theta/\partial x^1 & \partial\theta/\partial x^2 \end{bmatrix} \tag{2}$$

The six local Cartesian coordinate systems (x^1, x^2) that span the surface of the sphere (Fig.1) are based on equiangular central projection ([16, 17]) in such a way that $x^1 = x^1(\lambda, \theta)$, $x^2 = x^2(\lambda, \theta)$, and $-\pi/4 \leq x^1, x^2 \leq \pi/4$.

2.1 Shallow Water Equations

We consider the flux form shallow-water equations in curvilinear coordinates as described in Sadourny [19]. The governing equations for an inviscid flow of a thin layer of fluid in 2D are the horizontal momentum and continuity equations for the height h. Here, h is considered as the depth of the fluid and it is related to the free surface geopotential height (above sea level) $\Phi = g\,(h_s + h)$, where h_s denotes height of the underlying mountains and g is the gravitational acceleration.

In curvilinear coordinates, the continuity and momentum equations for the shallow water system may

be written as follows ([19, 17]),

$$\frac{\partial}{\partial t}(\sqrt{G}\,h) + \frac{\partial}{\partial x^1}(\sqrt{G}\,u^1 h) + \frac{\partial}{\partial x^2}(\sqrt{G}\,u^2 h) = 0, \tag{3}$$

$$\frac{\partial u_1}{\partial t} + \frac{\partial}{\partial x^1}E = \sqrt{G}\,u^2(f+\zeta), \tag{4}$$

$$\frac{\partial u_2}{\partial t} + \frac{\partial}{\partial x^2}E = -\sqrt{G}\,u^1(f+\zeta), \tag{5}$$

where

$$E = \Phi + \frac{1}{2}\,(u_1\,u^1 + u_2\,u^2), \quad \zeta = \frac{1}{\sqrt{G}}\left[\frac{\partial u_2}{\partial x^1} - \frac{\partial u_1}{\partial x^2}\right],$$

$f = 2\omega\,\sin\theta$ is the Coriolis parameter and ω is the rotation rate of the earth.

The system (3-5) may be expressed in the following flux form,

$$\frac{\partial}{\partial t}\mathbf{U} + \frac{\partial}{\partial x^1}\mathbf{F}_1(\mathbf{U}) + \frac{\partial}{\partial x^2}\mathbf{F}_2(\mathbf{U}) = \mathbf{S}(\mathbf{U}), \tag{6}$$

where $\mathbf{U} = \left[\sqrt{G}\,h, u_1, u_2\right]^T$, $\mathbf{F}_1 = \left[\sqrt{G}hu^1, E, 0\right]^T$ $\mathbf{F}_2 = \left[\sqrt{G}hu^2, 0, E\right]^T$, with the source term $\mathbf{S} = \left[0, \sqrt{G}u^2(f+\zeta), -\sqrt{G}\,u^1(f+\zeta)\right]^T$.

3 Discontinuous Galerkin Formulation

For simplicity, we proceed with a scalar component of (6) to describe the DG discretization.

$$\frac{\partial U}{\partial t} + \nabla\cdot\vec{\mathcal{F}}(U) = S(U), \quad \text{in} \quad \mathcal{D}\times(0,T), \tag{7}$$

for all $(x^1, x^2) \in \mathcal{D}$ with initial condition $U_0(x^1, x^2) = U(x^1, x^2, t=0)$. In (7), $\vec{\mathcal{F}} = (F_1, F_2)$ is the flux function, $U = U(x^1, x^2, t)$ and $\nabla \equiv (\partial/\partial x^1, \partial/\partial x^2)$ is the gradient operator.

The computational domain $\mathcal{D}$ is the surface of the cubed-sphere, spanning six identical non-overlapping subdomains (faces) such that $\mathcal{D} = \bigcup_{\nu=1}^{6}\Omega^\nu$. Therefore, it is only necessary to consider the discretization for a single subdomain Ω and the procedure can be analogously extended to the remaining subdomains. Consider a subdomain Ω which is partitioned into $N_e \times N_e$ rectangular non-overlapping elements Ω_{ij}; $i, j = 1, 2, \ldots, N_e$, such that

$$\Omega_{ij} = \{(x^1, x^2)\,|\,x^1 \in [x^1_{i-1/2}, x^1_{i+1/2}],\ x^2 \in [x^2_{j-1/2}, x^2_{j+1/2}]\}. \tag{8}$$

Thus, the total number of elements on the cubed sphere is $M = 6 \times N_e^2$.

The size of an element Ω_{ij} is determined by $\Delta x^1_i = (x^1_{i+1/2} - x^1_{i-1/2})$ and $\Delta x^2_j = (x^2_{j+1/2} - x^2_{j-1/2})$ in the x^1 and x^2-directions, respectively. For $t > 0$, consider an element Ω_{ij} in the partition of Ω and an approximate solution $U_h = U_h(x^1, x^2, t)$ belongs to the finite dimensional space $\mathcal{V}_h(\Omega)$. Multiplication of (7) by a test function $\varphi_h = \varphi_h(x^1, x^2) \in \mathcal{V}_h$ and integration over the element Ω_{ij} results in a weak Galerkin formulation of the problem.

$$\frac{\partial}{\partial t}\int_{\Omega_{ij}} U_h\,\varphi_h\,d\Omega - \int_{\Omega_{ij}} \mathcal{F}(U_h)\cdot\nabla\varphi_h\,d\Omega + \int_{\partial\Omega_{ij}} \mathcal{F}(U_h)\cdot\vec{n}\,\varphi_h\,ds = \int_{\Omega_{ij}} S(U_h)\,\varphi_h\,d\Omega, \tag{9}$$

where $\vec{n}$ is the outward-facing unit normal vector on the element boundary $\partial\Omega_{ij}$.

Along the boundaries of an element (internal interfaces) $\partial\Omega_{ij}$, the function U_h is discontinuous and the boundary integral (third term in (9)) is not uniquely defined. Therefore, the analytic flux $\mathcal{F}(U_h)\cdot\vec{n}$ in (9) must be replaced by a numerical flux $\widehat{\mathcal{F}}\,(U_h^-, U_h^+)$. The numerical flux resolves the discontinuity along the element edges and provides the only mechanism by which adjacent elements interact. For simplicity, the Lax-Friedrichs numerical flux as considered in [16, 17] is chosen for the present study, given by

$$\widehat{\mathcal{F}}(U_h^-, U_h^+) = \frac{1}{2}\left[(\mathcal{F}(U_h^-) + \mathcal{F}(U_h^+))\cdot\vec{n} - \alpha(U_h^+ - U_h^-)\right], \tag{10}$$

where U_h^- and U_h^+ are the left and right limits of the discontinuous function U_h evaluated at the element interface, α is the upper bound for the absolute value of eigenvalues of the flux Jacobian $\mathcal{F}'(U)$ in the direction $\vec{n}$. For the shallow-water system (6), the local maximum values of α in x^1 and x^2-directions for each element Ω_{ij} are defined as ([17]), $\alpha^1 = \max\left(|u^1| + \sqrt{\Phi\, G^{11}}\right)$, $\alpha^2 = \max\left(|u^2| + \sqrt{\Phi\, G^{22}}\right)$. Treatment of flux terms and vector quantities at the cube-face edges needs special attention, and it is discussed in [16].

3.1 Discretization

For each element Ω_{ij}, define the local variables $\xi^k = 2(x^k - x_i^k)/\Delta x_i^k$, where $x_i^k = (x_{i+1/2}^k + x_{i-1/2}^k)/2$, and $k = 1, 2$ denote the x^1, x^2-directions, respectively. By using these relations, an element Ω_{ij} is mapped onto the reference element $\widetilde{\Omega}_{ij} \equiv [-1, 1] \otimes [-1, 1]$.

An important aspect of the DG discretization is the choice of an appropriate set of basis functions (polynomials) that span $\mathcal{V}_h$. Nair et al. [16, 17] have used *modal* expansion basis, however, for the present work we use a high-order *nodal* basis set due to its computational efficiency. The choice of a particular type of basis is problem dependent and their relative merits are discussed in [12]. The nodal basis set is constructed using Lagrange-Legendre polynomials ($h_\ell(\xi^k)$) with roots at Gauss-Lobatto quadrature points.

In the two-dimensional (2D) (ξ^1, ξ^2) coordinate system, the test function (φ_h) as well as the the approximate solution U_h are expanded in terms tensor-product functions from the basis set. Thus,

$$U(\xi^1, \xi^2) = \sum_{\ell=0}^{N} \sum_{m=0}^{N} U_{\ell m}\, h_\ell(\xi^1)\, h_m(\xi^2) \quad \text{for} \quad -1 \le \xi^1, \xi^2 \le 1 \tag{11}$$

where

$$h_\ell(\xi^k) = \frac{(\xi^k - 1)(\xi^k + 1)\, L_N'(\xi^k)}{N(N+1)\, L_N(\xi_\ell^k)\, (\xi^k - \xi_\ell^k)}, \quad k \in \{1, 2\} \tag{12}$$

and $L_N(\xi^k)$ is the Legendre polynomial of degree N. The weak formulation (9) is simplified by mapping the elements onto the reference element, and utilizing (11). The final approximation of (7) takes the form,

$$\frac{d}{dt} U_{\ell m} = \mathcal{L}(U), \tag{13}$$

which is an ordinary differential equation (ODE) and can be solved using a variety of methods. Note that right side of Eq. (13) consists of both surface and boundary integrals, and these integrals are computed with an accurate Gauss-Lobatto-Legendre (GLL) quadrature rule.

3.2 Time Integration

The semi-discretized equation (13) for the shallow water system it takes the following form

$$\frac{d}{dt}\, \mathbf{U} = \mathbf{L}(\mathbf{U}) \quad \text{in} \quad (0, T). \tag{14}$$

Time integration of the SW equations can be performed by solving the system of ODEs (14). Total variation diminishing Runge-Kutta (TVD-RK) schemes do not introduce spurious oscillations for smooth problems and are widely used for solving (14) in the DG discretization [8]. For the present study we use the third-order TVD-RK scheme considered in [17] (without a limiter or a filter) and is written as follows for (14).

$$\begin{aligned}
\mathbf{U}^{(1)} &= \mathbf{U}^n + \Delta t\, \mathbf{L}(\mathbf{U}^n) \\
\mathbf{U}^{(2)} &= \frac{3}{4}\mathbf{U}^n + \frac{1}{4}\mathbf{U}^{(1)} + \frac{1}{4}\Delta t\, \mathbf{L}(\mathbf{U}^{(1)}) \\
\mathbf{U}^{n+1} &= \frac{1}{3}\mathbf{U}^n + \frac{2}{3}\mathbf{U}^{(2)} + \frac{2}{3}\Delta t\, \mathbf{L}(\mathbf{U}^{(2)}),
\end{aligned} \tag{15}$$

where the superscripts n and $n+1$ denote time levels t and $t + \Delta t$, respectively.

4 Numerical Results

Our DG scheme has been extensively tested using various initial conditions. Williamson et al. [23] proposed a suite of standard tests for the shallow water equations on the sphere. These idealized tests of varying complexity include experiments with north-south symmetry, balanced steady-state flows and extreme gradients.

We have employed a variety of grid systems with $M \times N_g \times N_g$ grid points, where M is the total number of elements ($M = 6N_e^2$) on the cubed-sphere and each element consists of $N_g \times N_g$ Gauss-Lobatto Legendre points. Numerical solutions produced with the DG scheme on the cubed-sphere are bilinearly interpolated onto a 128×65 longitude-latitude grid (approximately equal to the T42 resolution) for visualization.

4.1 Steady State Geostrophic Flow

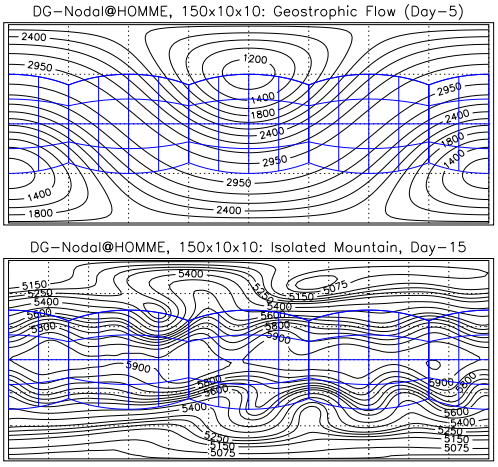

Figure 2: *Numerical solution for SW test case 2 (top panel) and for test case 5 (bottom panel). A cubed-sphere with 150 elements each containing* 10×10 *GLL points, is used for numerical integration.*

First, we consider test case 2 in [23], which is a steady-state solution of the full nonlinear SW equations. The wind field is uniform as in the solid-body rotation case and the equations are geostrophically balanced during the time evolution. The initial velocity and height fields are,

$$\begin{aligned} u &= u_0 \left(\cos\alpha_0 \cos\theta + \sin\alpha_0 \cos\lambda \sin\theta\right), \\ v &= -u_0 \sin\alpha_0 \sin\lambda, \\ g\,h &= g\,h_0 - \frac{u_0}{2}(2\,a\,\omega + u_0)\left(\sin\theta \cos\alpha_0 - \cos\lambda \cos\theta \sin\alpha_0\right)^2 \end{aligned}$$

a is the earth's radius, $u_0 = 2\pi a/(12 \text{ days})$, and $gh_0 = 2.94 \times 10^4 \text{ m}^2/\text{ s}^2$.

We have chosen the flow orientation parameter $\alpha_0 = \pi/4$, making the test more challenging on the cubed-sphere. Figure 2 shows the height and wind fields after 5 days of integration (upper panel). The experiment was performed on a $150 \times 10 \times 10$ grid (i.e., $N_e = 5, N_g = 10$) with time step $\Delta t = 36$ seconds.

4.2 Zonal Flow Over an Isolated Mountain

The second experiment we consider is test case 5 in [23], zonal flow over an isolated mountain. This test is particularly useful for studying the effectiveness of the scheme in conserving integral invariants such as mass, total energy and potential enstrophy. It consists of a zonal flow impinging on a mountain, and no analytic solution is known for this test. The center of the mountain is located at $(3\pi/2, \pi/6)$ with height $h_s = 2000\,(1 - r/R)$ meters, where $R = \pi/9$ and $r^2 = \min[R^2, (\lambda - 3\pi/2)^2 + (\theta - \pi/6)^2]$. The wind velocity and height fields are the same as in the previous case with $\alpha_0 = 0$, $gh_0 = 5960 \text{ m}^2/\text{s}^2$ and $u_0 = 20$ m/s.

Figure 3 (left panel) shows numerical results on a low-order $864 \times 4 \times 4$ grid. The numerical solutions are smooth (no spurious oscillations are observed) and they appear very similar to the high resolution spectral T213 solutions shown in [11]. However, the spectral solutions exhibit spurious oscillations in the vicinity of the mountain at all resolutions.

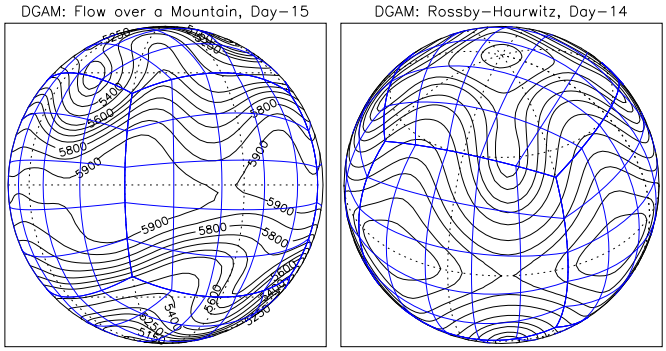

Figure 3: *Numerical solution for SW test case 5 (left panel) and for test case 6 (right panel). A cubed-sphere with 864 elements and each of which containing* 4×4 *GLL points, is used for numerical integration.*

4.3 Rossby-Haurwitz Wave

The third experiment is test case 6 in [23], a zonal wavenumber 4 Rossby-Haurwitz wave. The initial state is an exact steadily propagating solution of the nondivergent barotropic vorticity equation, but not an exact solution of the full SW system.

Figure 3 (right panel) shows numerical solution after 14 days of integration. A $864 \times 4 \times 4$ grid was employed which provides resolution somewhere between T42 and T63 of a spectral model. Unlike the NCAR spectral model, the DG scheme does not employ any diffusion terms. Nair et al. [17] have shown that for this experiment, the change in total energy is almost one order lower than a finite-volume SW model [14] and the potential enstrophy error (from initial value) is of the same magnitude.

5 Code Development, Tuning, and Performance

Development time was substantially reduced by building the model in the High Order Method Modeling Environment (HOMME) [9] developed at NCAR. This environment was originally designed to support the spectral element method on the cubed-sphere and has been extended to provide the basic building blocks necessary for rapid development of parallel high-order atmospheric models. In adopting this environment we also leverage previous and current work. For example, the ability to configure for shallow water and primitive equations (hydrostatic), support for various explicit and semi-implicit time-stepping schemes, efficient implementation of computational kernels, proven scaling to 1000's of processors [15], METIS [13] and space-filling curve partitioning [4], interfaces to physics packages, and support for geometrically non-conforming elements and adaptive meshes.

The modifications required to build a discontinuous Galerkin shallow water model in HOMME were minor, and do not impact parallel scalability. The existing HOMME communication framework consists of three different phases: packing, boundary exchange, and unpacking. The pack routine edgeVpack() copies data from the element data space into a communication buffer. The routine bndry_exchange() exchanges data between neighboring MPI processes. The unpack routine edgeVunpack() performs a direct stiffness summation of the data from the communication buffer back to element space. Two additional routines, edgeDGVpack() and edgeDGVunpack(), were added to support DG within the existing framework. The packing routine edgeDGVpack() is identical to the existing edgeVpack() and is provided for naming consistency. The routine edgeDGVunpack() replaced the existing direct stiffness summation with a data copy into a padded element data structure. The padded data structure contains field values for the element as well as a halo of the surrounding elements. The padded data structure is then provided to the DG flux computation.

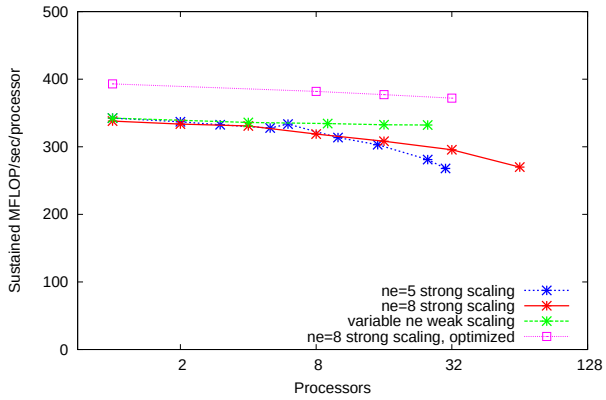

Figure 4: *Sustained MFLOP per second per processor for fixed total work (strong scaling) and fixed work per processor (weak scaling) tests.*

To assess performance we consider shallow water test case 2. For the strong scaling experiments we used cubed-spheres with 150 elements ($N_e = 5$) and 384 elements ($N_e = 8$). For the weak scaling experiment we varied the number of elements on a face such that there were 150 elements per processor. All tests were performed using 10×10 GLL points (i.e., 9^{th} order Legendre polynomials). Target system is a 132 processor Linux cluster. The system consists of 66 nodes (64 compute nodes and 2 head nodes). Compute nodes contain two 2.4 GHz Intel P4 Xeon processors with 2 GB RAM and are embedded in a Dolphin 8 x 8 torus network. Intel 8.0 compilers and ScaliMPI were used to build the application. SSE2 instructions were *not* enabled so theoretical CPU peak is 2.4 GFLOPS. Initial performance results show sustained performance for all three tests is between 268 and 342 MFLOPS (11-14% of peak). Though the scaling observed is quite good, sustained performance is lower than anticipated. One contributing factor is that we had not done *any* tuning. Another contributing factor is that test case 2 is a 2D problem. The sister SE primitive equation implementation in HOMME (quasi-3D) achieves approximately 20% of peak on IBM Power 3 systems and experience with a 3D spectral element code indicate that 30% of peak is obtainable for slightly larger polynomial degrees [22]. After one round of tuning, where we performed basic loop re-ordering and loop unrolling, sustained performance increased to approximately 16% of peak for the ($N_e = 8$) strong scaling case.

Through our partnership with IBM Research we were able to run on a four rack (8096 processor) IBM BlueGene/L system. Though initial performance results are promising, we were unable to complete the study in time for this publication.

6 Summary and Conclusions

The Discontinuous Galerkin transport scheme proposed by Nair et al. [16] has been further extended to the full set of nonlinear flux form shallow water equations on the sphere. The computational domain is the cubed-sphere, where a sphere is decomposed into six identical regions obtained by central (gnomonic) equiangular projections of the faces of the inscribed cube onto the spherical surface. The DG discretization employs a high-order nodal basis set consisting of Legendre polynomials and fluxes along the boundaries of the elements are approximated by a Lax-Friedrichs scheme. A third-order total variation diminishing Runge-Kutta scheme has been used for time integration, without any filter or limiter. The model has been validated using the standard test suite proposed by Williamson et al. [23].

The nodal DG scheme exhibits exponential convergence for SW test case two (steady state geostrophic flow problem). The DG solutions to the SW test cases are much better than those of a spectral model [11] for a given spatial resolution. Even with high-order spatial discretization, the solutions do not exhibit spurious oscillations for the flow over a mountain test case. Conservation of integral invariants has also been compared with existing finite-volume models (e.g., [14]). Our model conserves mass to machine precision, and although the scheme does not formally conserve global invariants such as total energy and potential enstrophy, conservation of these quantities is better preserved than in lower order finite-volume

models. Import of the DG model into the NCAR HOMME framework is complete and preliminary performance and scaling results are promising.

Acknowledgments

This work is supported by the DOE SciDAC program under award #DE-FG02-04ER63870. NCAR is sponsored by the National Science Foundation. This material is based upon work supported by the National Science Foundation under Grant No. 0325041. Computer time was provided by NSF ARI Grant #CDA-9601817, NSF MRI Grant #CNS-0420873, NASA AIST grant #NAG2-1646, and IBM.

References

[1] Cockburn, B., and C. W. Shu, 1989: TVB Runge-Kutta local projection discontinuous Galerkin method for conservation laws II: General framework. *Math. Comput.*, **52**, 411-435.

[2] Cockburn, B., and C. W. Shu, 1998: The Runge-Kutta discontinuous Galerkin finite element method for conservation laws V: Multidimensional systems. *J. Comput. Phy.*, **141**, 199-224.

[3] Cockburn, B., and C. W. Shu, 2001: The Runge-Kutta discontinuous Galerkin method for convection-dominated problems. *J. Sci. Computing*, **16**, 173-261.

[4] Dennis, J. M., 2003: Partitioning with Space-Filling Curves on the Cubed-Sphere, IPDPS'03, Nice, France.

[5] Fournier, A., M. A. Taylor, and J. J. Tribbia, 2004: A spectral element atmospheric model (SEAM): high-resolution parallel computation and localized resolution of regional dynamics. *Mon. Wea. Rev.*, **132**, 726-748.

[6] Giraldo, F. X., J. S. Hesthaven, and T. Warburton, 2003: Nodal high-order discontinuous Galerkin methods for spherical shallow water equations. *J. Comput. Phys.*, **181**, 499-525.

[7] Giraldo, F. X., and T. E. Rosmond, 2004: A scalable spectral element Eulerian atmospheric model (SEE-AM) for NWP: dynamical core test. *Mon. Wea. Rev.*, **132**, 133-153.

[8] Gottlieb, S., C. W. Shu, and E. Tadmor, 2001: Strong stability-preserving high-order time discretization methods. *SIAM Review*, **43**, 89-112.

[9] High Order Method Modeling Environment (HOMME), http://www.homme.ucar.edu/.

[10] Iskandrani, M., D. B. Haidvogal, J. C. Levin, E. Curchister, and C. A. Edwards, 2002: Multiscale geophysical modeling using the spectral element method. *Computing in Sci. and Eng.*, **4**, 42-48.

[11] Jakob-Chien, R., J. J. Hack, and D. L. Williamson, 1995: Spectral transform solutions to the shallow water test set. *J. Comput. Phys.*, **119**, 164-187.

[12] Karniadakis G. E., and S. J. Sherwin, 1999: *Spectral/hp Element Methods for CFD*. Oxford University Press, 1999.

[13] Karypis, G., and V. Kumar, 2004: METIS Family of Multilevel Partitioning Algorithms, http://www-users.cs.unm.edu/ karypis/metis/.

[14] Lin, S-J., and B. Rood, 1997: An explicit flux-form semi-Lagrangian shallow water model on the sphere. *Q. J. Roy. Met Soc.*, **123**, 2531-2533.

[15] Loft, R. D., S. J. Thomas, and J. M. Dennis, 2001: Terascale spectral element dynamical core for atmospheric general circulation models. Supercomputing 2001, ACM/IEEE conference, November 2001, Denver.

[16] Nair, R. D., S. J. Thomas, and R. D. Loft, 2005: A discontinuous Galerkin transport scheme on the cubed-sphere. *Mon. Wea. Rev.* in press.

[17] Nair, R. D., S. J. Thomas, and R. D. Loft, 2005: A discontinuous Galerkin global shallow water model. *Mon. Wea. Rev.* in press.

[18] Ronchi, C., R. Iacono, and P. S. Paolucci, 1996: The "Cubed Sphere" : A new method for the solution of partial differential equations in spherical geometry. *J. Comput. Phys.*, **124**, 93-114.

[19] Sadourny, R., 1972: Conservative finite-difference approximations of the primitive equations on quasi-uniform spherical grids. *Mon. Wea. Rev.*, **100**, 136-144.

[20] Taylor, M., J. Tribbia, and M. Iskandrani, 1997: The spectral element method for the shallow water equations on the sphere. *J. Comput. Phys.*, **130**, 92-108.

[21] Thomas, S. J., and R. D. Loft, 2002: Semi-implicit spectral element model. *J. Scientific Comput.*, **17**, 339-350.

[22] Tufo, H. M., Fischer, P. F., 1999: Terascale spectral element algorithms and implementations, Supercomputing 1999, IEEE/ACM conference, November 1999, Portland.

[23] Williamson, D. L., J. B. Drake, J. Hack, R. Jakob, and P. N. Swartztrauber, 1992: A standard test set for numerical approximations to the shallow water equations in spherical geometry. *J. Comput. Phys.*, **102**, 211-224.